## Advanced Nanomaterials

# NIR-OLED structures based on lanthanide coordination compounds: synthesis and luminescent properties

Artem Barkanov[1], Anna Zakharova[1], Tatjana Vlasova[1], Ekaterina Barkanova[1],
Andrew Khomyakov[1], Igor Avetissov[1,*] , Ilya Taydakov[2,3], Nikolay Datskevich[2],
Victoria Goncharenko[2,4], and Roman Avetisov[1]

[1] *Mendeleev University of Chemical Technology, Moscow, Russia*

[2] *P. N. Lebedev Physical Institute of the Russian Academy of Sciences, Moscow, Russia*

[3] *Department of Innovational Materials and Technologies Chemistry, Plekhanov Russian University of Economics, Moscow, Russia 117997*

[4] *Chemistry Department, Lomonosov Moscow State Univeristy, Moscow, Russia*

## ABSTRACT

Electroluminescence complexes based on ytterbium and 5-methyl-2-phenyl-4-(2,2,2-trifluoroacetyl)-2,4-dihydro-3H-pyrazol-3-one (HL) ligand and various diimine-type ancillary ligands (2,2-bipyridine, bathophenanthroline, 1,10-phenanthroline) have been synthesized, and corresponding crystals were investigated. [Yb(L)$_3$(bipy)] and [Yb(L)$_3$(bath)] complexes have triclinic structure (P-1), while [Yb(L)$_3$(phen)] complex has orthorhombic structure (P2$_1$2$_1$2$_1$). The crystallography parameters were determined. The photoluminescence of the complexes demonstrated only bands resulted from $^2F_{5/2} \rightarrow ^2F_{7/2}$ transition and corresponding three Stark subcomponents generated due to the crystal field action. NIR-OLED structures with emitting layers based on the [Yb(L)$_3$(bipy)], [Yb(L)$_3$(bath)], and [Yb(L)$_3$(phen)] complexes have been fabricated, and their electroluminescence demonstrated maxima intensities at 978 and 1005 nm. Comparison of NIR-OLEDs power density showed that the maximal power densities of 2.17 (978 nm) and 1.92 (1005 nm) $\mu$W $\times$ cm$^{-2}$ were determined for the NIR-OLED based on [Yb(L)$_3$(bath)] complex.

---

Springer

## Introduction

Nowadays, there is a growing interest in emitters in the near-infrared region. According to ISO 20473 scheme, the infrared region is divided into three bands of near-infrared (NIR) radiation (780–3000 nm), mid-infrared radiation (3–50 mm), and far-infrared radiation (50 mm–1 mm) [1].

The capabilities of organic light-emitting diodes in their configuration and efficiency leave them far ahead of inorganic competitors. It is already known about the use of NIR-OLED in wireless data transmission devices [2], medicine (e.g., pulse oximeters [3]), night vision and data storage devices [4], and other applications [5, 6]. However, there are not so many emitters of this spectral range and OLEDs based on them; therefore, research in this area is increasing along with the growing popularity of OLEDs themselves.

The most popular in the production of organic light-emitting diodes are derivatives of d-metals, primarily of the platinum group (iridium [7], platinum, osmium), and some compounds of light elements, for example, aluminum. Although platinum and especially iridium complexes exhibit excellent luminescent properties, they are not without significant disadvantages. First of all, it is the price and availability of platinum group metals. To date, it has become obvious that at the same rate of consumption in the near future, the reserves of iridium will be exhausted [8]. The second problem is that, due to the electroluminescence mechanism, which is mainly due to emission from charge transfer triplet states (3MLCT), it is practically impossible to obtain emitters that are efficient for the near-infrared region. The few examples of compounds which demonstrated electroluminescence in the near-infrared range, as a rule, have comparatively low efficiency in the wavelength region of 750–850 nm, with further efficiency decrease at longer wavelength [9]. One of the solutions to the described disadvantages is the use of coordination compounds of rare earth elements—lanthanides.

Lanthanide coordination compounds are of a great importance for modern technology and science. For example, they are extensively used in advanced photonics, optoelectronics, and spectroscopy [10–12].

Among all emitting lanthanide ions, $Nd^{3+}$, $Er^{3+}$, and $Yb^{3+}$ are of special interest due to NIR emission in the range of 880–1600 nm. The $Yb^{3+}$ ion has a single emission peaked around 980 nm originated from the $^2F_{5/2} \rightarrow {}^2F_{7/2}$ transition. The NIR emission from the Yb(III) ion is used in biomedical imaging, because it is long-lived and because it has higher efficiency compared to the other NIR-emitting Ln(III) ions [10, 13].

Pyrazole-substituted 1,3-diketones and especially 4-acylpyrazolenes are unique class of chelating ligands, which were used previously for preparation of highly-luminescent lanthanide complexes [14–19]. A drawback of many of the reported conventional diketone-based lanthanide complexes is that their visible, and in particular, NIR emission is often efficiently quenched by the vibrational overtones of CH bonds within the sensitizing ligands. This process can be suppressed by the preparation of fully fluorinated or deuterated organic ligands [20], or by excluding high-energy vibrating bonds in close proximity to the emitting $Ln^{3+}$ center [13, 21]. The pyrazolone core is containing small number of such bonds, and in addition, an introduction of perfluorinated substituents in side chain can additionally reduce quenching. With all that said, 5-methyl-2-phenyl-4-(2,2,2-trifluoroacetyl)-2,4-dihydro-3H-pyrazol-3-one (HL) seems to be a good candidate for preparation of bright luminescent complexes with $Ln^{3+}$ ions and different ancillary ligands.

Some complexes of 5-methyl-2-phenyl-4-(2,2,2-trifluoroacetyl)-2,4-dihydro-3H-pyrazol-3-one (HL) with selected lanthanides [22–24], $VO^{2+}$ [25], $Cu^{2+}$ [26, 27], $Ag^+$[26], $Ph_3Sn$[28, 29], $Sr^{2+}$[23], and other metals [30–32] were reported previously. To date, none of the obtained lanthanide complexes of the ligand HL were tested in OLED devices, although some of them were found to be string luminescent in solid phase or in the polymer films [22, 24].

In the present research, we report on synthesis and systematic investigation of electroluminescent properties for a series of $Yb^{3+}$ with 5-methyl-2-phenyl-4-(2,2,2-trifluoroacetyl)-2,4-dihydro-3H-pyrazol-3-one (HL) and different diimine ancillary ligands (1,10-phenanthroline, 2,2-bipyridine and 4,7-diphenyl-1,10-phenanthroline).

## Experimental section

### General remarks

Ytterbium (III) chloride hexahydrate (99.99%), gadolinium (III) chloride hexahydrate (99.99%), and other reagents were purchased from Aldrich and used without additional purification. 5-Methyl-2-phenyl-2,4-dihydro-3H-pyrazol-3-one was obtained from phenylhydrazine and ethyl 3-oxobutanoate according known synthetic procedure [33].

#### Elemental analysis and NMR spectroscopy

Elemental analyses were performed on an Elemental Vario MicroCube CHNO(S) analyzer. Metal content was determined by complexometric titration with Trilon B solution in the presence of xylenol orange as an indicator. Complexes were decomposed before analysis by heating with concentrated $HNO_3$. $^1H$ and $^{19}F$ NMR spectra were recorded at 300 K on a Bruker AM-300 instrument operating at 300.12 and 282.4 MHz for $^1H$ and $^{19}F$ nucleus, respectively. Chemical shifts were reported in ppm with respect to internal standard TMS ($\delta = 0.00$ ppm) or external standard $CFCl_3$ ($\delta = 0.00$ ppm).

#### Optical adsorption

Optical absorption spectra for the complexes and free ligand were measured in solutions in 1-cm-path-length quartz cells. The samples were dissolved in acetonitrile (SuperGradient grade, Panreac, Spain) with a concentration of about $1 \times 10^{-5}$ mol/L. Optical absorption spectrum was registered at room temperature with the use of a Jasco V-770 spectrophotometer with a 200–900-nm operational range.

#### Luminescent measurements

Photoluminescent steady-state spectra at an ambient temperature were measured by an Ocean Optics Maya Pro CCD spectrometer operating within 200–1100 nm spectral range. Powdered samples were placed in 4-mm O.D. quartz tubes for measurements. CW laser diode (370 nm) with appropriate band-pass filter was used as an excitation source. Optical fibers with appropriate quartz optics were used for illumination of the sample and collection of emitting light. Low-temperature phosphorescent spectrum of

complex **4** was recorded on a Varian Cary Eclipse spectrofluorimeter operated at 250–900 nm spectral range. Xe-flash lamp was used as an excitation source, and powdered sample (in a sealed 4-mm O.D. quartz-glass tube) was placed in custom-made quartz-glass cryostat, filled with liquid $N_2$. An appropriate delay (80–100 μs) between flash of the lamp and data collection was used in order to exclude any residual fluorescence. All data were corrected on instrument response function.

#### X-ray analysis

Single X-ray diffraction analysis was carried out on a Bruker D8 Quest diffractometer (MoKα radiation, $\omega$- and $\varphi$-scan mode). The structures were solved with direct methods and refined by least-squares method in the full-matrix anisotropic approximation on $F^2$. Crystal of $[Yb(L)_3(phen)]$ (**1**) is a racemic twin with fractions 0.89/0.11. All hydrogen atoms were located in calculated positions and refined within riding model. All calculations were performed using the SHELXTL [34, 35] and Olex2 [36] software packages. Atomic coordinates, bond lengths, angles, and thermal parameters have been deposited at the Cambridge Crystallographic Data Centre with deposition numbers—CCDC 2,098,196, 2,098,197, and 2,098,198, which are available free of charge at www.ccdc.cam.ac.uk.

### Synthesis of ligand and complexes

#### Preparation of 5-methyl-2-phenyl-4-(2,2,2-trifluoroacetyl)-2,4-dihydro-3H-pyrazol-3-one (HL).

The ligand HL was obtained by a modification of procedure, described earlier by Jensen [37] (Scheme 1). Briefly, to a solution of 12.8 g (73 mmol) of 5-methyl-2-phenyl-2,4-dihydro-3H-pyrazol-3-one in 80 mL of dry pyridine 10 mL (72 mmol, 15 g) of trifluoroacetic anhydride was added dropwise with
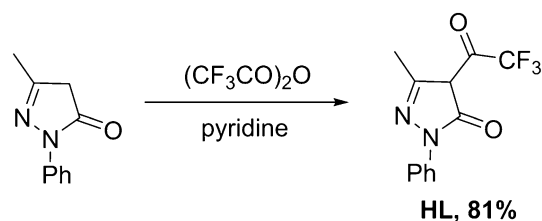


**Scheme 1** Preparation of the ligand **HL**.

magnetic stirring in such a rate to maintain temperature below 40 °C (cold water bath). After addition, dark red–brown solution was stirred at a room temperature for 2 h and poured into 300 mL of cold water with stirring. The solution was made acidic by carefully addition of conc. HCl until precipitation of the diketone was completed. The resulted precipitate was filtered off, washed by water until neutral pH of filtrate was reached and dried in air to a constant weight. It was further purified by recrystallization of hot EtOH–water mixture. Yield was 15.7 g (81%) of light greenish powder. M.p. 142–143 °C (lit. 144 °C for keto form [37]).

Calc. for $C_{12}H_9F_3N_2O_2$ (270.20): C, 53.34; H, 3.36; N, 10.37%; found: C, 53.29; H, 3.48; N, 10.30%.

$^1$H-NMR (300 MHz, CDCl$_3$): δ (ppm): 7.80 (d, 2H, Ph), 7.50 (t, 2H, Ph), 7.37 (t, 1H, Ph), 2.48 (d, 3H, CH$_3$).
$^{19}$F-NMR (300 MHz, CDCl$_3$): δ (ppm): −75.55.

## Preparation of Yb complexes 1–3 and Gd complex 4.

A solution of 0.405 g (1.5 mmol) of ligand HL in 10 mL of ethanol was placed in a borosilicate glass vial with a screw cap (PTFE septa) and heated to 40 °C with magnetic stirring (Scheme 2). Corresponding diimine ligand (0.5 mmol, 0.078 g of 2,2-bipyridyl, 0.090 g of 1,10-phenanthroline or 0.166 g of bathophenanthroline) was added, and stirring was continued until clear solution was formed. Hot solution of 0.194 g (0.5 mmol) YbCl$_3$·6H$_2$O in 2 mL of EtOH was then added followed by dropwise addition of 1.5 mL 1 M solution of NaOH in EtOH. The resulted mixture was kept in a closed vial for 2 h at 40 °C and left overnight at a room temperature. The resulted precipitates were filtered off, washed successively with 2 mL of 50% aqueous EtOH, 5 mL of deionized water and 5 mL of pentane and dried at 40 °C and 0.1 torr to a constant weight.

[Yb(L)$_3$(phen)] (1).
White powder. Yield was 0.447 g (77%).
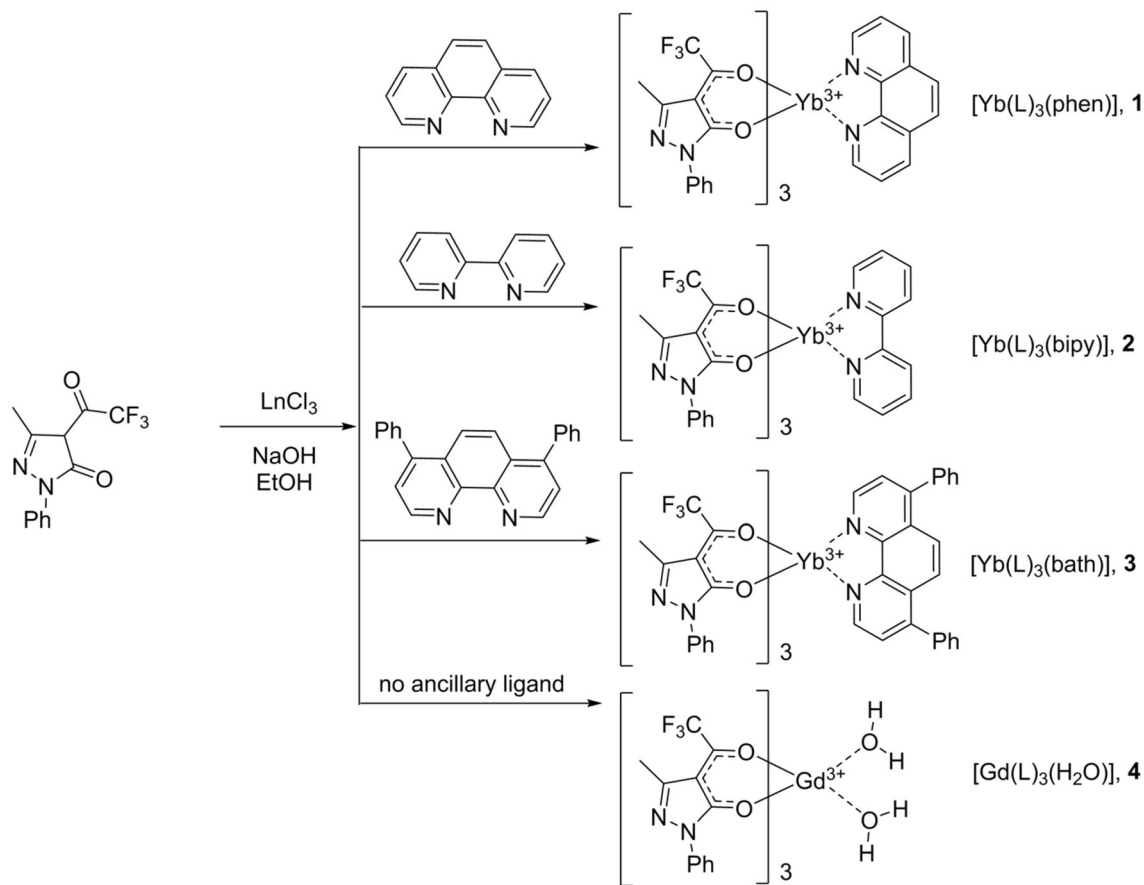


**Scheme 2** Preparation of complexes.

Calc. for $C_{48}H_{32}F_9N_8O_6Yb$ (1160.84): C, 49.66; H, 2.78; N, 9.65; Yb, 14.91%; found: C, 49.73; H, 2.82; N, 9.69; Yb, 15.01%.

$[Yb(L)_3(bipy)]$ (**2**).
White powder. Yield was 0.392 g (69%).
Calc. for $C_{46}H_{32}F_9N_8O_6Yb$ (1136.82): C, 48.60; H, 2.84; N, 9.86; Yb, 15.22%; found: C, 48.66; H, 2.89; N, 9.80; Yb, 15.32%.

$[Yb(L)_3(bath)]$ (**3**).
White powder. Yield was 0.551 g (84%).
Calc. for $C_{60}H_{40}F_9N_8O_6Yb$ (1313.03): C, 54.88; H, 3.07; N, 8.53; Yb, 13.18%; found: C, 54.91; H, 3.12; N, 8.60; Yb, 13.35%.

Complex $[Gd(L)_3(H_2O)_2]$ (**4**) was obtained in the similar way, stating from 0.405 g (1.5 mmol) of ligand HL and 0.186 g (0.5 mmol) $GdCl_3*6H_2O$.
Yield was 0.265g (53 %) of Greenish powder. Yield was 0.265 g (53%).
Calc. for $C_{36}H_{28}F_9GdN_6O_8$ (1000.88): C, 43.20; H, 2.82; N, 8.40; Gd, 15.71%; found: C, 43.27; H, 2.89; N, 8.38; Gd, 15.90%.

## OLED fabrication and testing

Multilayers OLED devices were fabricated by layer-by-layer vacuum thermal deposition ($< 10^{-6}$ torr) on glass substrates (20 × 30 × 1.1 mm, RMS = 2.3 nm, LT-G001 ITO Glass 15Ω, from Lumtec Corp.) with ITO (indium tin oxide) conducting layer as anode. Extra pure $MoO_3$ (99.9995 wt% free of W impurity) was used as a hole blocking material [38]. NPB (N,N′-di(1-naphthyl)-N,N′-diphenyl-(1,1′-biphenyl)-4,4′-diamine) was used as one of the most efficient hole-transport materials to provide the necessary hole mobility [38, 39]. Bebq$_2$ (bis(10-hydroxy-benzo[h]quinolinato)beryllium) was used as host matrix and as electron transport material for phosphorescent dopants. Aluminum was used as cathode material. The deposition rates of each organic layer did not exceed 0.03 nm × s$^{-1}$ to obtain the most homogeneous films. To measure the electroluminescence (EL) parameters of the fabricated OLED structures, they were encapsulated in a special cell filled with argon. A GPD-73303D (Good Will Instrument Co., Taiwan) was used as a power source for OLED structures.

The electroluminescence (EL) of OLED structures was activated by a direct current, which is determined by an applied voltage and structure resistivity.

OLED structures were tested using a LumiCam 1300 photometer–colorimeter (Instrument Systems Optische Messtechnik, GmbH, Germany) to study the uniformity of radiation distribution. Spectral measurements were carried out using an Ocean Optics NIRQuest-512 spectrophotometer in the wavelength range of 900–1700 nm with an integration time of 1000 ms. An Optical Power Meter model 1830-R with an 818-IG silicon detector with an operating wavelength range of 800 to 1650 nm (Newport Corporation, USA) was used as an optical power meter. Current–voltage characteristics were measured using a GDM-78261 universal digital voltmeter (Good Will Instrument Co., Taiwan).

## Results and discussion

### X-ray structures of complexes

Pale yellow crystals of complexes **1–3**, suitable for X-ray diffraction experiments, were obtained by slow evaporation of solutions in EtOH at room temperature. Selected crystallographic data and refinement details for complexes **1–3** are listed in Table 1.

All three structures were monomolecular complexes (Fig. 1). The ytterbium ion is coordinated by three diketonate ligands, and the coordination environment is saturated by two nitrogen atoms of the diimine ligands. Coordination number of Yb$^{3+}$ is equal to eight in all cases, and coordination polyhedron {YbO$_6$N$_2$} can be best described as distorted square antiprism. Ytterbium bond lengths with the atoms forming its coordination polyhedron are listed in Table 2.

The crystal packing analysis revealed an existence of weak intermolecular interactions of the C–H…F type. Average H…F distances are 2.56, 2.58, and 2.49 Å for complexes **1–3**, respectively. Further analysis of the $[Yb(L)_3(bipy)]$ packing revealed the presence of a series of π-stacking interactions of bipyridyl ligands with each other, as well as stacking interactions of the phenyl substituent and the pyrazole ring of the diketonate ligands (Fig. 2). For complexes **1** and **3**, weak interactions of the C–H… π type between the diimine ligand and the pyrazole ring of the diketonate ligand were observed.

**Table 1** Crystallographic data and refinement details for complexes 1–3

| Parameter | Value | | |
|---|---|---|---|
| | [Yb(L)$_3$(bipy)] | [Yb(L)$_3$(phen)] | [Yb(L)$_3$(bath)] |
| Molecular formula | C$_{46}$H$_{32}$F$_9$N$_8$O$_6$Yb | C$_{48}$H$_{32}$F$_9$N$_8$O$_6$Yb | C$_{60}$H$_{40}$F$_9$N$_8$O$_6$Yb |
| M | 1136.83 | 1160.85 | 1313.04 |
| Temperature, K | 100(2) | 110(2) | 110(2) |
| System | Triclinic | Orthorhombic | Triclinic |
| Space group | P-1 | P2$_1$2$_1$2$_1$ | P-1 |
| $a$, Å | 11.8681(3) | 10.5581(8) | 12.4824(16) |
| $b$, Å | 13.5862(4) | 18.6780(16) | 14.4887(16) |
| $c$, Å | 14.8048(4) | 22.6536(19) | 15.5174(18) |
| $\alpha$, deg | 91.9160(10) | 90 | 82.905(2) |
| $\beta$, deg | 111.5110(10) | 90 | 82.012(2) |
| $\gamma$, deg | 95.1250(10) | 90 | 77.5150(10) |
| V, Å$^3$ | 2206.36(11) | 4467.4(6) | 2700.7(6) |
| Z | 2 | 4 | 2 |
| $\rho_{calc}$, g/cm$^3$ | 1.711 | 1.726 | 1.615 |
| $\mu$(Mo$K_\alpha$), mm$^{-1}$ | 2.218 | 2.193 | 1.824 |
| $F$(000) | 1126 | 2300 | 1310 |
| θmin–θmax, deg | 1.51–30.00 | 2.103–29.00 | 1.98–25.00 |
| Number of measured reflections | 35,371 | 17,578 | 15,515 |
| Number of unique reflections ($R_{int}$) | 12,838 (0.0292) | 17,578 (0.0681) | 9359 (0.0246) |
| Number of reflections with $I > 2\sigma(I)$ | 12,051 | 15,944 | 8705 |
| Number of refined parameters | 634 | 653 | 760 |
| R-factors ($I > 2\sigma(I)$) | $R_1 = 0.0238$, $\omega R_2 = 0.0536$ | $R_1 = 0.0548$, $\omega R_2 = 0.1225$ | $R_1 = 0.0356$, $\omega R_2 = 0.0825$ |
| R-factors (all reflections) | $R_1 = 0.0265$, $\omega R_2 = 0.0545$ | $R_1 = 0.0633$, $\omega R_2 = 0.1273$ | $R_1 = 0.0391$, $\omega R_2 = 0.0843$ |
| GOOF | 1.065 | 1.049 | 1.055 |
| $\Delta\rho_{max}$ / $\Delta\rho_{min}$, e/Å$^3$ | 1.717 / − 0.687 | 2.022 / − 1.120 | 2.576 / − 1.590 |

Comparison of XRD patterns of powder preparations with those simulated on the basis of single-crystal crystallographic data (Figs. S4-S6) showed the satisfactory coincidence, which indicated the prepared powders were well crystallized and their phase purities were close to those of single crystals. The chemical purity of the synthesized complexes was determined by ICP–MS analysis (Table S1). The corresponding values of chemical purity of 99.996 wt% for Yb(L)$_3$(bipy), 99.990 wt% for Yb(L)$_3$(phen), and 99.988 wt% for Yb(L)$_3$(bath) were determined.

## Photophysical properties and energy transfer diagram for 1–3

The photophysical properties of the free ligand HL and its complexes 1–3 have been examined in dilute MeCN solution at room temperature and are summarized in Table 3 and Fig. 4. As shown in Fig. 3, similar ligands-centered solution absorption spectra

were observed in the UV region. These bands were associated with $^1\pi$–$\pi^*$ and $^1\pi$–n transitions in the organic ligands. One can see that additional bands in spectra of complexes 1–3 are redshifted with respect to absorption maxima in spectra of free ligand HL. They can be attributed to the absorption of diimine ligands.

All three complexes 1–3 were demonstrated specific NIR luminescence of Yb$^{3+}$ upon UV (370 nm) excitation. The organic ligands acted as antennas [40], which absorbed light and transferred the energy to the Yb$^{3+}$ ion. The only one transition ($^2F_{5/2} \rightarrow {}^2F_{7/2}$) in Yb$^{3+}$ was observed, corresponding to a relatively broad emission band peaked around 1006 nm. Due to relatively unsymmetrical ligand environment, the band was split into three subcomponents as a result of ligand field interaction of Yb$^{3+}$ ion (Fig. 4).

To analyze energy transfer pathways in details, low-temperature phosphorescence (77 K) spectrum of gadolinium complex 4 was recorded. Since the

**Figure 1** General view of complexes 1 **a**, 2 **b**, and 3 **c**. Atoms are represented as thermal ellipsoids at 50% probability. Hydrogen atoms are omitted for clarity.
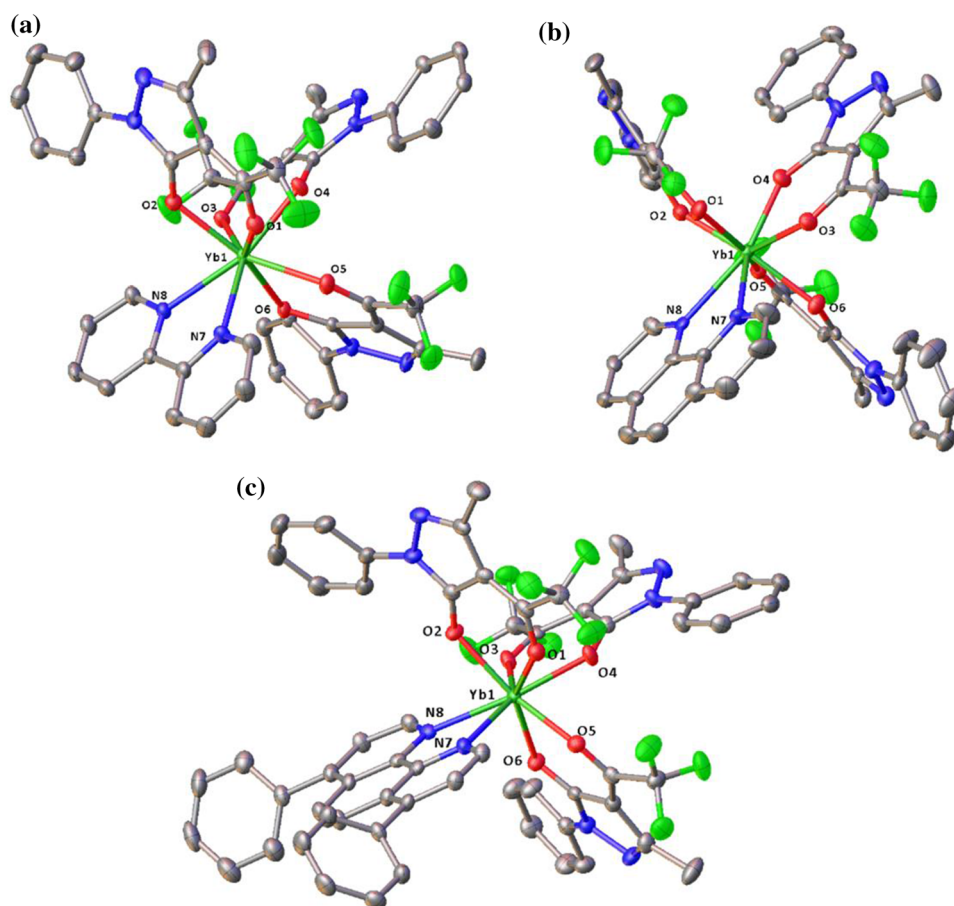


**Table 2** Bond lengths in the coordination polyhedra of ytterbium in complexes 1–3

| Yb—X | Bond length, Å | | |
|---|---|---|---|
| | [Yb(L)$_3$(bipy)] | [Yb(L)$_3$(phen)] | [Yb(L)$_3$(bath)] |
| Yb1–O1 | 2.3131(14) | 2.300(7) | 2.335(3) |
| Yb1–O2 | 2.2381(14) | 2.275(7) | 2.233(3) |
| Yb1–O3 | 2.3348(13) | 2.361(7) | 2.352(3) |
| Yb1–O4 | 2.2289(13) | 2.243(8) | 2.238(3) |
| Yb1–O5 | 2.3554(14) | 2.376(7) | 2.326(3) |
| Yb1–O6 | 2.2779(14) | 2.217(7) | 2.217(3) |
| Yb1–N7 | 2.4769(16) | 2.519(9) | 2.479(3) |
| Yb1–N8 | 2.5012(16) | 2.490(9) | 2.503(3) |



**Figure 2** π–π stacking interactions in the crystal of [Yb(L)$_3$(bipy)](2). Hydrogen atoms are omitted for clarity.

Gd$^{3+}$ ion has no energy levels below 32,000 cm$^{-1}$ and therefore cannot accept any energy from the excited state of the ligand [41] at low temperature, complex 4 exhibits the typical phosphorescence ($\lambda_{em}$ = 532 nm), from which the triplet ($^3\pi$–$\pi^*$) energy level (18,832 cm$^{-1}$) was calculated. For ancillary ligands
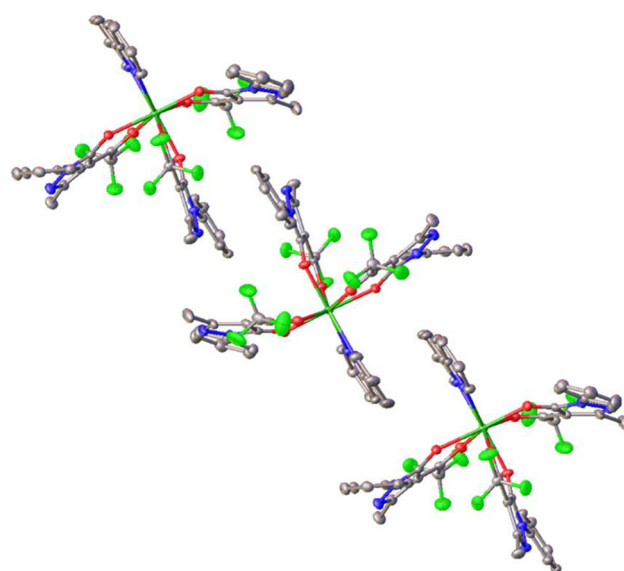
bipy (23,148 cm$^{-1}$), phen (21,645 cm$^{-1}$) [42] and bath (22,000 cm$^{-1}$) [43] triplet ($^3\pi$–$\pi^*$) energy level had

**Table 3** Photophysical properties of HL and complexes 1–3 in MeCN solutions

| Compound | $\lambda_{max}$, nm ($cm^{-1}$) | Extinction, $M^{-1} \times cm^{-1}$ |
|---|---|---|
| HL | 234 (42,735) | 153,000 |
| | 278 (35,971) | 134,452 |
| [Yb(L)$_3$(bipy)] | 244(40,983) | 592,970 |
| | 283(35,335) | 583,915 |
| [Yb(L)$_3$(phen)] | 229(43,668) | 546,445 |
| | 250(40,000) | 444,025 |
| | 271(36,900) | 461,820 |
| | 292(34,246) | 346,900 |
| [Yb(L)$_3$(bath)] | 220(45,454) | 668,210 |
| | 243(41,152) | 634,190 |
| | 281(35,587) | 760,050 |
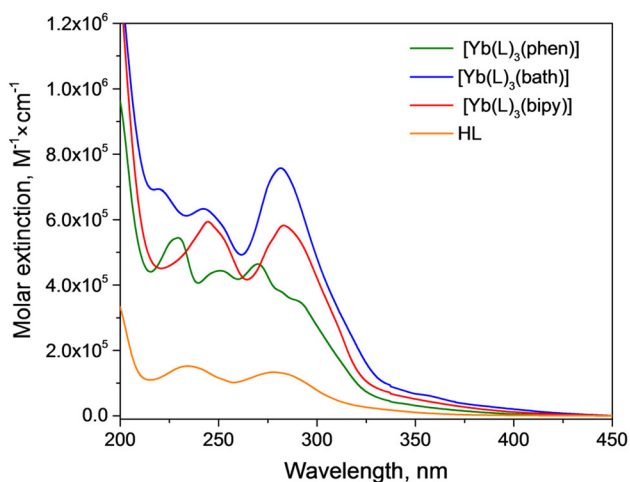


**Figure 3** Absorption spectra of free ligand HL and complexes 1–3 in MeCN solutions.
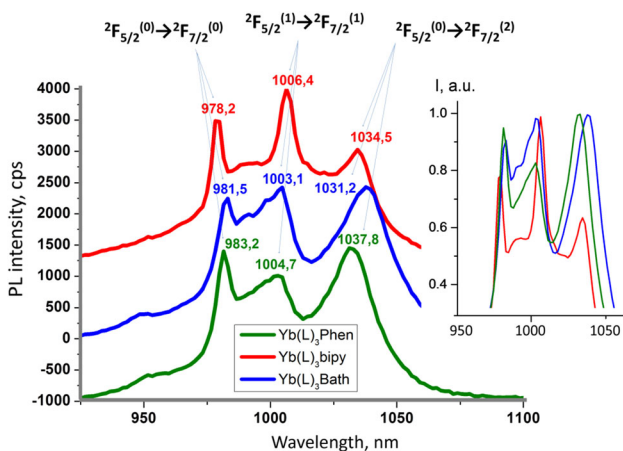


**Figure 4** Emission spectra of 1–3 complexes ($\lambda^{ext}$ = 370 nm) with corresponding Stark splitting.

been measured previously. The energies of singlet levels ($^1\pi$–$\pi^*$) of the ligands were estimated from observed absorption spectra.

The simplified energy transfer diagram for complexes 1–3 is presented in Fig. 5. Since the energy gap between first triplet level ($T_1$) of the ligand HL and resonant level $^2F_{5/2}$ of the Yb$^{3+}$ (10,400 cm$^{-1}$, [44]) ion is the smallest ($\sim$ 8430 cm$^{-1}$), the energy transfer from this $T_1$ level is much probable than from $T_1$ levels of ancillary ligands. Nevertheless, the role of ancillary ligands is not limited by saturation of inner coordination sphere of Yb$^{3+}$. Less effective but yet important pathways of the central ion sensibilization may include an interligand energy transfer and other less common processes. Unfortunately, since the energy gap between $T_1$ and $^2F_{5/2}$ levels is sufficiently large, a noticeable quenching of luminescence by multiphonon relaxation was observed. This process is typical for the most of Yb$^{3+}$ diketonates and leads to a significant decrease in total quantum yields of photoluminescence [45]. The detailed energy transfer mechanism for given complexes is currently under investigation.
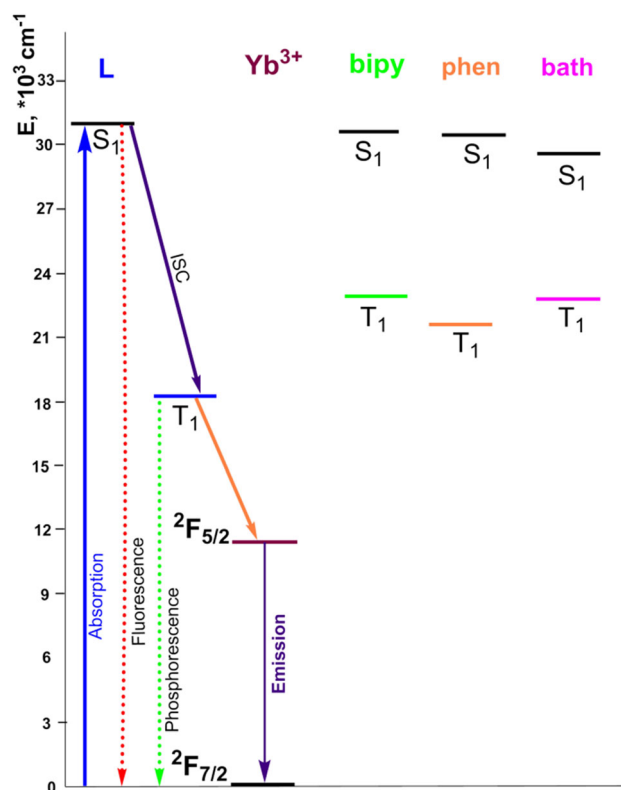


**Figure 5** Simplified energy transfer diagram for complexes 1–3. The possible energy transfer pathways from ancillary ligands are not shown for clarity.

## OLED performance

OLED devices were fabricated and examined to test the suitability of synthesized substances as emissive materials for NIR-OLED application. The topology of the manufactured OLEDs was as follows: ITO/ MoO$_3$ (1 nm)/ NPB (40 nm)/Bebq$_2$: X (20 nm)/Bebq$_2$ (40 nm)/LiF (1.2 nm)/ Al, where X is:

Yb(L)$_3$(bipy) for **1** structure,
Yb(L)$_3$(phen) for **2** structure,
Yb(L)$_3$(bath) for **3** structure.

All the devices obtained showed electroluminescence in the near-infrared range (Fig. 6). The maximum of the luminescence spectra was specific for ytterbium compounds and corresponded to the following values:

978 nm, 1006 nm, and 1034 nm for **1** structure;
978 nm, 1005 nm, and 1034 nm for **2** structure;
978 nm, 1005 nm, and 1031 nm for **3** structure.

The obtained EL spectra practically did not differ from each other. However, the differences are more noticeable when comparing the PL spectra with the EL spectra of the corresponding complexes and OLED structures on their basis (Fig. 7). For all OLED structures, we observed the strong reduction in EL intensity of $^2F_{5/2}^{(0)} \rightarrow {}^2F_{7/2}^{(2)}$ subcomponent transition compared to the PL of crystalline complexes. This could be explained by different stacking of crystalline structures and complexes materials in the thin-film OLED structures as well as the AC electric field action.
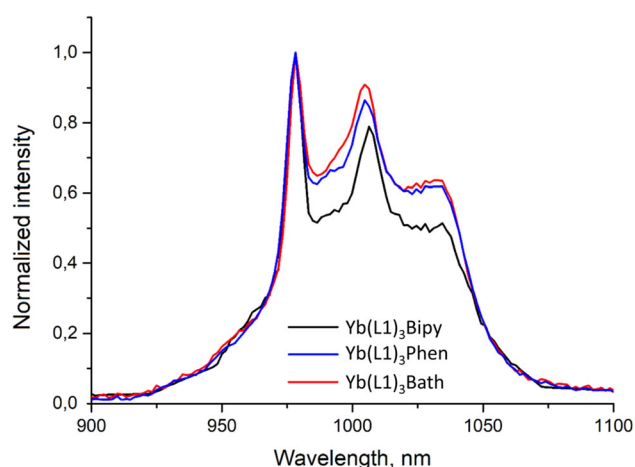


**Figure 6** Normalized PL spectra of OLEDs based on **1–3** complexes.

The usage of the well-known phosphorus Bebq$_2$ as a matrix material and an electron transport layer material, as expected, led to electroluminescence in the visible region of the spectrum. Despite this, the EL brightness was insignificant (about 2–4 cd × m$^{-2}$), but this allowed us to use the Lumi-Cam photometer–colorimeter to obtain 3D visualization of the brightness intensity distribution (Fig. 8). As can be seen from the image, the OLED structures turned out to be homogeneous.

All the fabricated devices based on the studied compounds revealed a characteristic nonlinear behavior of the *J–V* curves (Fig. 9). The turn-on voltages of NIR-OLEDs were ~ 5.5 V.

In order to obtain the most reliable values of the optical power, an IKS-1 light filter ($\lambda_{cutoff}$ = 750 nm) was added to the measuring benchmark, which was installed directly on the OLED structure. The obtained OLED characteristics, including optical power, are presented in Table 4.

Analysis of NIR-OLED power density of the structures based on various Yb-based emitting materials (Fig. 10) showed that the difference in power density at 978 and 1005 nm was not more than 20%. The maximal power density was observed for OLED based on Yb(L)$_3$(bath). This resulted from the better charge-transfer properties of the bathophenanthroline in comparison with 2,2-bipyridine and phenanthroline [46].

The obtained values are several times higher than those described earlier by Li and co-workers for ytterbium complexes based on simple diketones of the pyrazolone series. (At 977 nm, maximal irradiance of 0.14, 0.42, 0.8, and 1.47 μW × cm$^{-2}$ is described for various OLED topologies [47].) This became possible due to the optimization of the ligand structure; however, the OLED topology was not optimized in this case. It should be noted that more efficient platinum complexes, for example, do not allow reaching such long waves as lanthanides and do not have such narrow spectral lines. If we talk about the synthesis of more efficient quinolate emitters, then their synthesis requires isolation from air, since these adducts are unstable to water and oxygen, and requires special conditions for synthesis. At the moment, organic light-emitting diodes with ytterbium complexes are poorly studied, but our results are already a good contribution to their study, albeit without optimization of OLEDs.
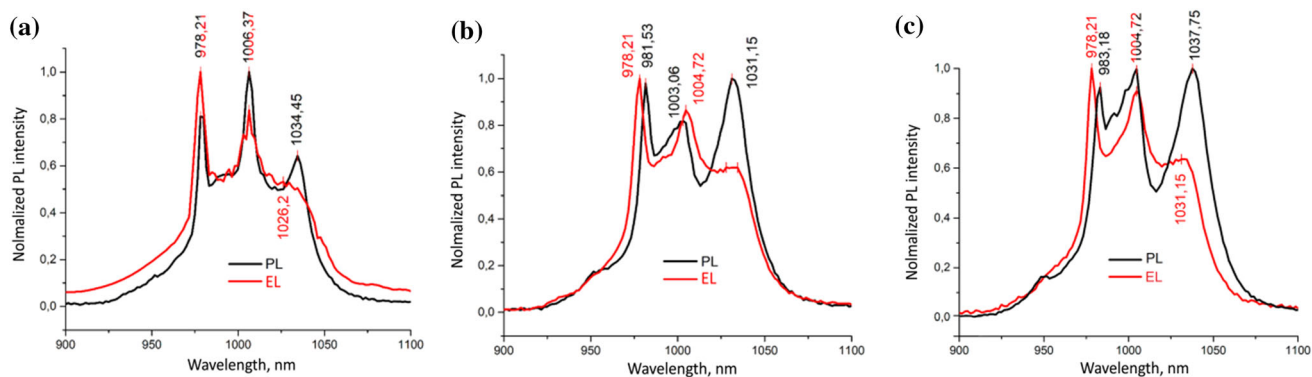
**Figure 7** Comparison of PL and EL spectra of crystalline **1 a**, **2 b**, and **3 c** complexes and OLED structures on their basis.
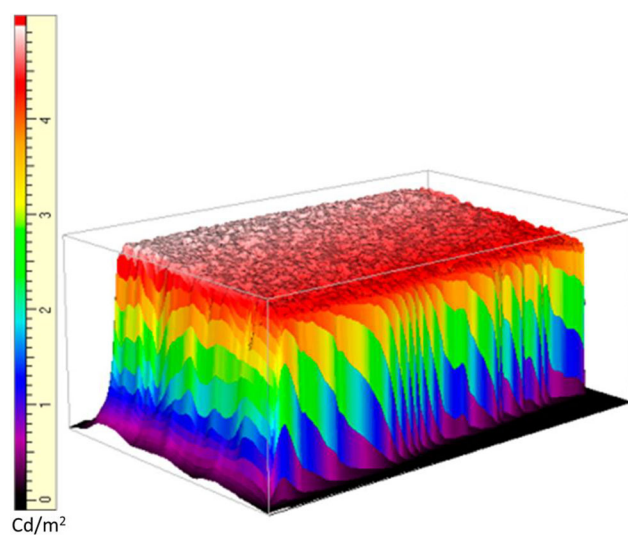


**Figure 8** 3D brightness mapping of the OLED structure based on complex **1**.

No direct correlation between Yb content in the active layer of OLED and its power density can be established, because the energy transfer to Yb ion is not straightforward. The efficiency of OLED is depending upon a superposition of various factors, including efficiency of excitons (triplet and singlet excitons are possible) formation, the position of recombination zone in the OLED structure, efficiency of energy transfer between triplet level of the ligands and Yb ion, various non-radiative processes, and many other factors. That is why it is hard to predict which complex will be a better emitter in OLED before carefully experimental evaluation of real structures [48].
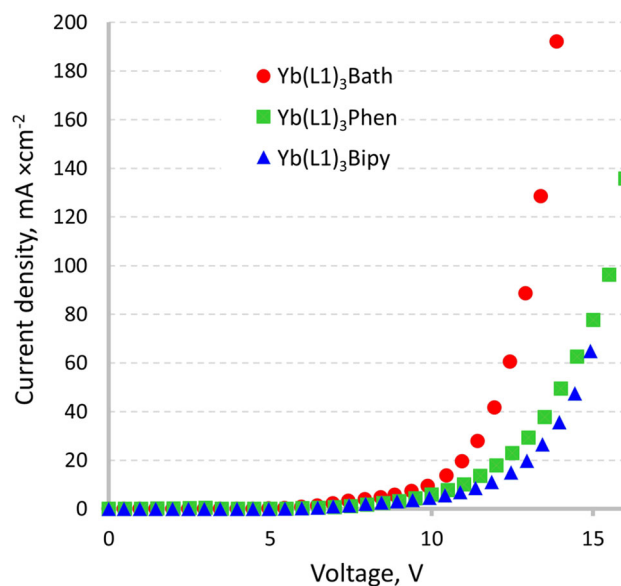


**Figure 9** Current density *vs* voltage dependence for the fabricated OLEDs.

## Conclusions

In conclusion, the pure complexes based on ytterbium and 5-methyl-2-phenyl-4-(2,2,2-trifluoroacetyl)-2,4-dihydro-3H-pyrazol-3-one (HL) ligand and various diimine ligands (2,2-bipyridine, bathophenanthroline, 1,10-phenanthroline) generating the antenna effect have been synthesized. The produced complexes were crystallized, and X-ray analysis showed that [Yb(L)$_3$(bipy)] and [Yb(L)$_3$(bath)] complexes were triclinic (P-1), while [Yb(L)$_3$(phen)] complex has orthorhombic structure (P2$_1$2$_1$2$_1$). The photoluminescence of the complexes demonstrated only bands resulted from $^2F_{5/2} \rightarrow {}^2F_{7/2}$ transition and corresponding three Stark subcomponents observing due to the crystal field action. NIR-OLED structures with

**Table 4** Characteristics of the fabricated NIR-OLED structures

| OLED Structure | 1 Structure | 2 Structure | 3 Structure |
|---|---|---|---|
| Emitting material | Yb(L)$_3$(bipy) | Yb(L)$_3$(phen) | Yb(L)$_3$(bath) |
| Turn-on voltage, V | 5.5 | 5.5 | 5 |
| Max. voltage, V | 15 | 16 | 14 |
| Max. power density at 14 V (at wavelength, nm), $\mu W \times cm^{-2}$ | 1.83 (978) | 2.04 (978) | 2.17 (978) |
| | 1.63 (1005) | 1.84 (1005) | 1.92 (1005) |
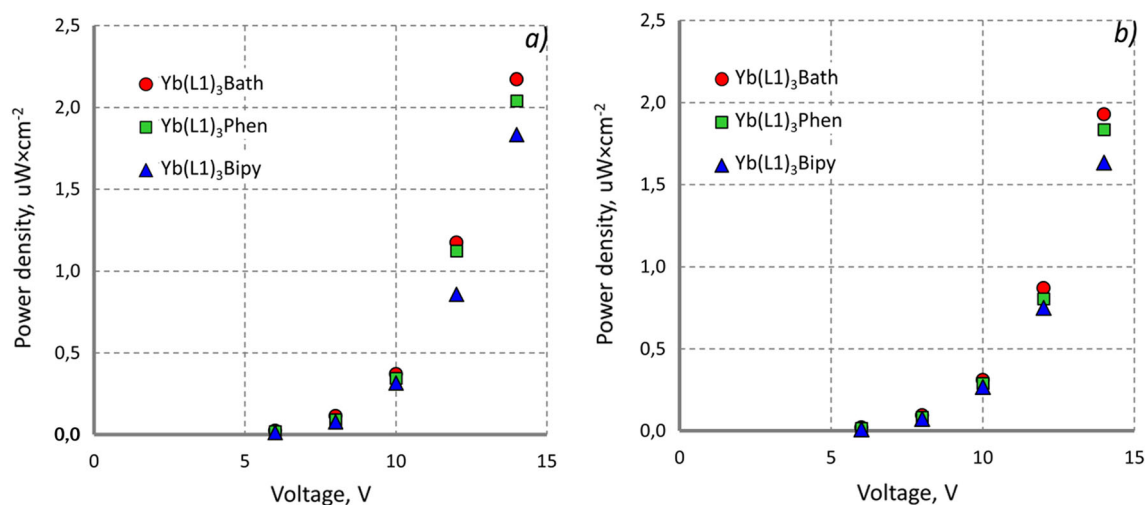


**Figure 10** Power density of 1–3 OLED structures at various voltages: at emission wavelength 978 nm **a** and 1005 nm **b**.

emitting layers based on the [Yb(L)$_3$(bipy)], [Yb(L)$_3$(bath)], and [Yb(L)$_3$(phen)] complexes demonstrated electroluminescence with maxima of 978 and 1005 nm. The maximal power densities of 2.17 (978 nm) and 1.92 (1005 nm) $\mu W \times cm^{-2}$ were determined for the OLED based on [Yb(L)$_3$(bath)].

## Acknowledgements

**Supplementary Information:** The online version contains supplementary material available at https://doi.org/10.1007/s10853-021-06721-4.

## References

[1]  ISO 20473 (2007) Optics and photonics — Spectral bands

[2]  Minotto A, Haigh PA, Łukasiewicz ŁG, Lunedei E, Gryko DT, Darwazeh I, Cacialli F (2020) Visible light communication with efficient far-red/near-infrared polymer light-emitting diodes. Light Sci Appl 9(1):1–11. https://doi.org/10.1038/s41377-020-0314-z

[3]  Lochner CM (2018) Printed organic light emitting diodes for biomedical applications. Doctoral dissertation, UC Berkeley

[4]  Smith AM, Mancini MC, Nie S (2009) Second window for in vivo imaging. Nat Nanotechnol 4(11):710–711. https://doi.org/10.1038/nnano.2009.326

[5]  Cao M, Wang X, Zhang M et al (2019) Electromagnetic response and energy conversion for functions and devices in low-dimensional materials. Adv Funct Mater 29:1807398. https://doi.org/10.1002/adfm.201807398

[6]  Yao L-H, Cao W-Q, Shu J-C et al (2021) Tailoring adsorption for tunable lithium ion storage and devices. Chem Eng J 413:127428. https://doi.org/10.1016/j.cej.2020.127428

[7]  Zhang Y, Qiao J (2021) Near-infrared emitting iridium complexes: molecular design, photophysical properties, and related applications. iScience 24:102858. https://doi.org/10.1016/j.isci.2021.102858

[8] Zysman-Colman E (ed) (2017) Iridium (III) in optoelectronic and photonics applications. John Wiley & Sons, Hoboken

[9] Ly KT, Chen-Cheng RW, Lin HW, Shiau YJ, Liu SH, Chou PT, Tsao C-S, Huang Y-C, Chi Y (2017) Near-infrared organic light-emitting diodes with very high external quantum efficiency and radiance. Nat Photonics 11(1):63–68. https://doi.org/10.1038/nphoton.2016.230

[10] Pushkarev AP, Bochkarev MN (2016) Organic electroluminescent materials and devices emitting in UV and NIR regions. Russ Chem Rev 85:1338–1368. https://doi.org/10.1070/RCR4665

[11] Fu G, Guan J, Li B et al (2018) An efficient and weak efficiency-roll-off near-infrared (NIR) polymer light-emitting diode (PLED) based on a PVK-supported Zn 2+ –Yb 3+ -containing metallopolymer. J Mater Chem C 6:4114–4121. https://doi.org/10.1039/C7TC05400A

[12] Bünzli J-CG (2015) On the design of highly luminescent lanthanide complexes. Coord Chem Rev 293–294:19–47. https://doi.org/10.1016/j.ccr.2014.10.013

[13] Santos HP, Gomes ES, dos Santos MV et al (2019) Synthesis, structures and spectroscopy of three new lanthanide β-diketonate complexes with 4,4′-dimethyl-2,2′-bipyridine. Near-infrared electroluminescence of ytterbium(III) complex in OLED. Inorganica Chim Acta 484:60–68. https://doi.org/10.1016/j.ica.2018.09.030

[14] Taydakov IV, Zaitsev BE, Krasnoselskiy SS, Starikova ZA (2011) Synthesis, X-ray structure and luminescent properties of Sm3+ ternary complex with novel heterocyclic β-diketone and 1,10-phenanthroline (Phen). J Rare Earths 29:719–722. https://doi.org/10.1016/S1002-0721(10)60529-7

[15] Metlin MT, Ambrozevich SA, Metlina DA et al (2017) Luminescence of pyrazolic 1,3-diketone Pr3+ complex with 1,10-phenanthroline. J Lumin 188:365–370. https://doi.org/10.1016/J.JLUMIN.2017.04.058

[16] Taidakov IV, Zaitsev BE, Lobanov AN et al (2013) Synthesis and luminescent properties of neutral Eu(III) and Gd(III) complexes with 1-(1,5-dimethyl-1h-pyrazol-4-yl)-4,4,4-trifluoro-1,3-butanedione and 4,4,5,5,6,6,6-heptafluoro-1-(1-methyl-1H-pyrazol-4-yl)-1,3-hexanedione. Russ J Inorg Chem 58:411–415. https://doi.org/10.1134/S0036023613040190

[17] Metlina DA, Metlin MT, Ambrozevich SA et al (2018) Luminescence and electronic structure of Nd3+ complex with pyrazole-substituted 1,3-diketone and 1,10-phenanthroline. J Lumin 203:546–553. https://doi.org/10.1016/J.JLUMIN.2018.07.005

[18] Gontcharenko VE, Kiskin MA, Dolzhenko VD et al (2021) Mono- and Mixed Metal Complexes of Eu3+, Gd3+, and Tb3+ with a Diketone, Bearing Pyrazole Moiety and CHF2-Group: structure, color tuning, and kinetics of energy transfer between lanthanide ions. Molecules 26:2655. https://doi.org/10.3390/molecules26092655

[19] Taydakov IV, Belousov YA, Lyssenko KA et al (2020) Synthesis, phosphorescence and luminescence properties of novel europium and gadolinium tris-acylpyrazolonate complexes. Inorganica Chim Acta 502:119279. https://doi.org/10.1016/j.ica.2019.119279

[20] George TM, Varughese S, Reddy MLP (2016) Near-infrared luminescence of Nd 3+ and Yb 3+ complexes using a polyfluorinated pyrene-based β-diketonate ligand. RSC Adv 6:69509–69520. https://doi.org/10.1039/C6RA12220E

[21] Reid BL, Stagni S, Malicka JM et al (2014) Lanthanoid β-triketonates: a new class of highly efficient NIR emitters for bright NIR-OLEDs. Chem Commun 50:11580–11582. https://doi.org/10.1039/C4CC04961F

[22] Zhang Z, Yu C, Liu L et al (2016) Efficient near-infrared (NIR) luminescent PMMA-supported hybrid materials doped with tris-β-diketone Ln3+ complex (Ln=Nd or Yb). J Photochem Photobiol A Chem 314:104–113. https://doi.org/10.1016/j.jphotochem.2015.08.022

[23] Marchetti F, Pettinari C, Pettinari R et al (2002) A new family of ionic dinuclear strontium (imH2)2[Sr2(Q)6] compounds (imH = imidazole; QH = 1-phenyl-3-methyl-4-acylpyrazol-5-one). J Chem Soc Dalt Trans. https://doi.org/10.1039/b200189f

[24] Zhang X, Liu L, Yu C et al (2016) Highly efficient near-infrared (NIR) luminescent tris- β -diketonate Yb 3+ complex in solution and in PMMA. Inorg Chem Commun 70:153–156. https://doi.org/10.1016/j.inoche.2016.06.006

[25] Cecchini MM, De Angelis F, Iacobucci C et al (2016) Mild catalytic oxidations of unsaturated fatty acid methyl esters (FAMEs) by oxovanadium complexes. Appl Catal A Gen 517:120–128. https://doi.org/10.1016/j.apcata.2016.01.045

[26] Marchetti F, Pettinari C, Pettinari R et al (2000) Influence of sterically demanding groups on the structure and stability in the solid and solution state of (acylpyrazolonate)bis(phosphine)copper(I) derivatives. Inorganica Chim Acta 299:65–79. https://doi.org/10.1016/S0020-1693(99)00463-6

[27] Golubev AS, Tyutin VY, Chkanikov ND et al (1992) Reactions of highly electrophilic polyfluoro unsaturated compounds with pyrazole derivatives. Bull Russ Acad Sci Div Chem Sci 41:2068–2073. https://doi.org/10.1007/BF00863375

[28] Marchetti F, Pettinari C, Cingolani A et al (1999) Tin(IV) and organotin(IV) derivatives of novel β-diketones. J Organomet Chem 580:344–353. https://doi.org/10.1016/S0022-328X(98)01173-5

[29] Bovio B, Cingolani A, Marchetti F, Pettinari C (1993) Tin(IV) and organotin(IV) complexes containing the anion

of some substituted-3-methyl-4-acyl-5-pyrazolones. Crystal structure of dimethylbis(1-phenyl-3-methyl-4-benzoyl pyrazolon-5-ato)tin(IV). J Organomet Chem 458:39–48. https://doi.org/10.1016/0022-328X(93)80455-K

[30] Okafor EC (1981) The metal complexes of heterocyclic β-diketones and their derivatives, part viii synthesis, structure, proton nmr and infrared spectral studies of the complexes of Al(III), Fe(III), Co(III), Rh(III), In(III), and Zr(IV) with l-phenyl-3-methyl-4-trifluoroa. Zeitschrift für Naturforsch B 36:213–217. https://doi.org/10.1515/znb-1981-0217

[31] Marchetti F, Pettinari C, Pettinari R et al (2007) Areneruthenium(II) 4-Acyl-5-pyrazolonate derivatives: coordination chemistry, redox properties, and reactivity. Inorg Chem 46:8245–8257. https://doi.org/10.1021/ic700394r

[32] Nagar MS, Ruikar PB, Subramanian MS (1988) Complexes of tetravalent plutonium, uranium and thorium with acylpyrazolones. Inorganica Chim Acta 141:309–312. https://doi.org/10.1016/S0020-1693(00)83925-0

[33] Deruiter J, Carter DA, Arledge WS, Sullivan PJ (1987) Synthesis and reactions of 4-isopropylidene-1-aryl-3-methyl-2-pyrazolin-5-ones. J Heterocycl Chem 24:149–153. https://doi.org/10.1002/jhet.5570240128

[34] Sheldrick GM (2015) SHELXT—Integrated space-group and crystal-structure determination. Acta Crystallogr Sect A Found Adv 71:3–8. https://doi.org/10.1107/S2053273314026370

[35] Sheldrick GM (2015) Crystal structure refinement with SHELXL. Acta Crystallogr Sect C Struct Chem 71:3–8. https://doi.org/10.1107/S2053229614024218

[36] Dolomanov OV, Bourhis LJ, Gildea RJ et al (2009) OLEX2: a complete structure solution, refinement and analysis program. J Appl Crystallogr 42:339–341. https://doi.org/10.1107/S0021889808042726

[37] Jensen BS, Meier H, Lundquist K, Refn S (1959) The Synthesis of 1-Phenyl-3-methyl-4-acyl-pyrazolones-5. Acta Chem Scand 13:1668–1670. https://doi.org/10.3891/acta.chem.scand.13-1668

[38] Buckley A (2013) Organic light-emitting diodes (OLEDs): materials, devices and applications, 1st edn. Woodhead Publishing, Sawston

[39] So F (2010) Organic electronics: materials, processing devices and applications. CRC Press, Francis and Taylor, Boca Raton

[40] Bünzli J-CG, Eliseeva SV (2010) Basics of lanthanide photophysics. In: Hänninen P, Härmä H (eds) Lanthanide luminescence. Springe, Berlin, pp 1–45

[41] Carnall WT, Fields PR, Rajnak K (1968) Electronic energy levels of the trivalent lanthanide Aquo Ions. II. Gd 3+. J Chem Phys 49:4443–4446. https://doi.org/10.1063/1.1669894

[42] Faustino WM, Malta OL, Teotonio EES et al (2006) Photoluminescence of europium(iii) dithiocarbamate complexes: electronic structure, charge transfer and energy transfer. J Phys Chem A 110:2510–2516. https://doi.org/10.1021/jp056180m

[43] Korshunov VM, Ambrozevich SA, Taydakov IV et al (2019) Novel β-diketonate complexes of Eu3+ bearing pyrazole moiety for bright photo- and electroluminescence. Dye Pigment 163:291–299. https://doi.org/10.1016/j.dyepig.2018.12.006

[44] Metlin MT, Goryachii DO, Aminev DF et al (2021) Bright Yb3+ complexes for efficient pure near-infrared OLEDs. Dye Pigment 195:109701. https://doi.org/10.1016/j.dyepig.2021.109701

[45] Rogozhin AF, Silantyeva LI, Yablonskiy AN et al (2021) Near infrared luminescence of Nd, Er and Yb complexes with perfluorinated 2-mercaptobenzothiazolate and phosphine oxide ligands. Opt Mater (Amst) 118:111241. https://doi.org/10.1016/j.optmat.2021.111241

[46] Taydakov IV, Akkuzina AA, Avetisov RI et al (2016) Effective electroluminescent materials for OLED applications based on lanthanide 1.3-diketonates bearing pyrazole moiety. J Lumin 177:31–39. https://doi.org/10.1016/j.jlumin.2016.04.017

[47] Li Z, Zhang H, Yu J (2012) Near-infrared electroluminescence from double-emission-layers devices based on Ytterbium (III) complexes. Thin Solid Films 520(9):3663–3667. https://doi.org/10.1016/j.tsf.2011.12.052

[48] Yersin H (2007) Highly efficient OLEDs with phosphorescent materials. Wiley-VCH Verlag GmbH & Co KGaA, Weinheim